REVIEW ARTICLE | FOCUS
PUBLISHED ONLINE: 27 NOVEMBER 2015 | DOI: 10.1038/NPHOTON.2010.201
nature photonics

Spin–orbit interactions of light

K. Y. Bliokh[1,2*], F. J. Rodríguez-Fortuño[3], F. Nori[1,4] and A. V. Zayats[3]

Light carries both spin and orbital angular momentum. These dynamical properties are determined by the polarization and spatial degrees of freedom of light. Nano-optics, photonics and plasmonics tend to explore subwavelength scales and additional degrees of freedom of structured — that is, spatially inhomogeneous — optical fields. In such fields, spin and orbital properties become strongly coupled with each other. In this Review we cover the fundamental origins and important applications of the main spin–orbit interaction phenomena in optics. These include: spin-Hall effects in inhomogeneous media and at optical interfaces, spin-dependent effects in nonparaxial (focused or scattered) fields, spin-controlled shaping of light using anisotropic structured interfaces (metasurfaces) and robust spin-directional coupling via evanescent near fields. We show that spin–orbit interactions are inherent in all basic optical processes, and that they play a crucial role in modern optics.

Light consists of electromagnetic waves that oscillate in time and propagate in space. Scalar waves are described by their intensity and phase distributions. These are the spatial (orbital) degrees of freedom common to all types of waves, both classical and quantum. In particular, a localized intensity distribution determines the position of a wave beam or packet, whereas the phase gradient describes the propagation of a wave (that is, its wavevector or momentum). Importantly, electromagnetic waves are described by vector fields[1]. Light therefore also possesses intrinsic polarization degrees of freedom, which are associated with the directions of the electric and magnetic fields oscillating in time. In the quantum picture, the right- and left-hand circular polarizations, with the electric and magnetic fields rotating about the wavevector direction, correspond to two spin states of photons[2].

Recently, there has been enormous interest in the spin–orbit interactions (SOI) of light[3–6]. These are striking optical phenomena in which the spin (circular polarization) affects and controls the spatial degrees of freedom of light; that is, its intensity distributions and propagation paths. The intrinsic SOI of light originate from the fundamental spin properties of Maxwell's equations[7,8] and, therefore, are analogous to the SOI of relativistic quantum particles[2,9,10] and electrons in solids[11,12]. As such, intrinsic SOI phenomena appear in all basic optical processes but, akin to the Planck-constant smallness of the electron SOI, they have a spatial scale of the order of the wavelength of light, which is small compared with macroscopic length scales.

Traditional 'macroscopic' geometrical optics can safely neglect the wavelength-scale SOI phenomena by treating the spatial and polarization properties of light separately. In particular, these degrees of freedom can be independently manipulated: by lenses or prisms, on the one hand, and polarizers or anisotropic waveplates, on the other. SOI phenomena come into play at the subwavelength scales of nano-optics, photonics and plasmonics. These areas of modern optics essentially deal with nonparaxial, structured light fields characterized by wavelength-scale inhomogeneities. The usual intuition of geometrical optics (based on the properties of scalar waves) does not work in such fields and should be substituted by the full-vector analysis of Maxwell waves. The SOI of light represent a new paradigm that provides physical insight and describes the behaviour of polarized light at subwavelength scales.

In the new reality of nano-optics, SOI phenomena have a two-fold importance. First, the coupling between the spatial and polarization properties must be taken into account in the analysis of any nano-optical system. This is absolutely essential in the conception and design of modern optical devices. Second, the SOI of light can bring novel functionalities to optical nano-devices based on interactions between spin and orbital degrees of freedom. Indeed, SOI provide a robust, scalable and high-bandwidth toolbox for spin-controlled manipulations of light. Akin to semiconductor spintronics, SOI-based photonics allows information to be encoded and retrieved using polarization degrees of freedom.

Below we overview the SOI of light in paraxial and nonparaxial fields, in both simple optical elements (planar interfaces, lenses, anisotropic plates, waveguides and small particles) and complex nano-structures (photonic crystals, metamaterials and plasmonics structures). We divide the numerous SOI phenomena into several classes based on the following most representative examples:

(1) A circularly polarized laser beam reflected or refracted at a planar interface (or medium inhomogeneity) experiences a transverse spin-dependent subwavelength shift. This is a manifestation of the spin-Hall effect of light[13–20]. This effect provides important evidence of the fundamental quantum and relativistic properties of photons[16,18], and it causes specific polarization aberrations at any optical interface. Supplied with suitable polarimetric tools, it can be employed for precision metrology[21,22].

(2) The focusing of circularly polarized light by a high-numerical-aperture lens, or scattering by a small particle, generates a spin-dependent optical vortex (that is, a helical phase) in the output field. This is an example of spin-to-orbital angular momentum conversion in nonparaxial fields[23–31]. Breaking the cylindrical symmetry of a nonparaxial field also produces spin-Hall effect shifts[32–37]. These features stem from fundamental angular-momentum properties of photons[8,38], and they play an important role in high-resolution microscopy[35], optical manipulations[25,26,39], polarimetry of scattering media[40,41] and spin-controlled interactions of light with nano-elements or nano-apertures[29,34,37,42,43].

(3) A similar spin-to-vortex conversion occurs when a paraxial beam propagates in optical fibres[44] or anisotropic crystals[45–47]. Most importantly, properly designing anisotropic and inhomogeneous structures (for example, metasurfaces or liquid crystals) allows considerable enhancement of the SOI effects

[1]Center for Emergent Matter Science, RIKEN, Wako-shi, Saitama 351-0198, Japan. [2]Nonlinear Physics Centre, RSPhysE, The Australian National University, Canberra, Australia. [3]Department of Physics, King's College London, Strand, London WC2R 2LS, UK. [4]Physics Department, University of Michigan, Ann Arbor, Michigan 48109-1040, USA. *e-mail: k.bliokh@gmail.com

Box 1 | Angular momenta of light.

Paraxial optical beams can carry three types of angular momentum (AM)[72–74]. First, the rotating electric and magnetic fields in a circularly polarized beam produce spin AM (SAM) **S**. SAM is aligned with the direction of propagation (momentum $\mathbf{P} = \langle\mathbf{k}\rangle$) of the beam and is determined by the polarization helicity $\sigma \in (-1, 1)$. The polarization helicity — the degree of circular polarization — is ±1 for right- and left-hand circular polarizations (as defined from the point of view of the source).

Second, optical vortex beams with helical wavefronts carry intrinsic orbital AM (IOAM) $\mathbf{L}^{\text{int}}$. Akin to SAM, IOAM is aligned with the momentum and is determined by the vortex topological charge $\ell = 0, \pm1, \pm2, \ldots$ (that is, the phase increment around the vortex core, modulo 2π).

Finally, beams propagating at a distance from the coordinate origin possess extrinsic orbital AM (EOAM) $\mathbf{L}^{\text{ext}}$. This is analogous to the mechanical AM of a classical particle and is given by the cross-product of the transverse position of the beam centre, $\mathbf{R} = \langle\mathbf{r}\rangle$, and its momentum **P**. These parameters characterize the trajectory of the beam and may vary in inhomogeneous media.

The above optical angular momenta are shown schematically in the figure, and are described by the following expressions (assuming values per photon in $\hbar = 1$ units):

$$\mathbf{S} = \sigma\frac{\mathbf{P}}{P}, \quad \mathbf{L}^{\text{int}} = \ell\frac{\mathbf{P}}{P}, \quad \mathbf{L}^{\text{ext}} = \mathbf{R}\times\mathbf{P}$$

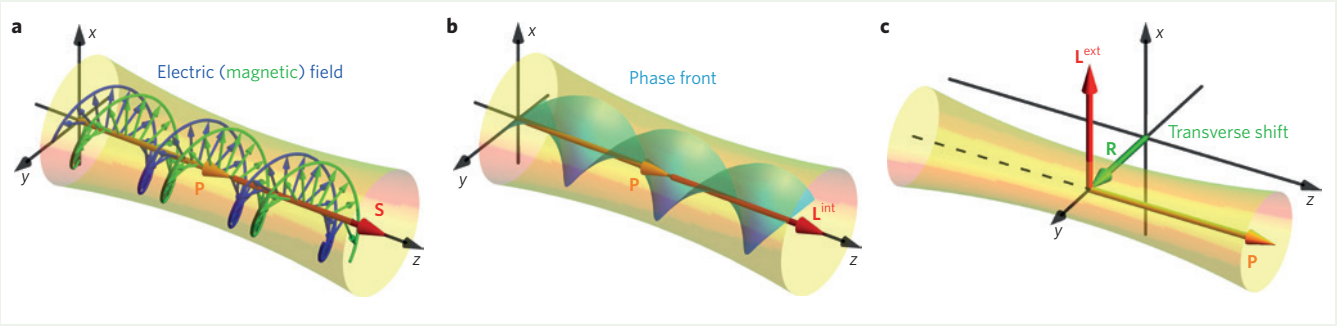

Angular momenta of paraxial optical beams. a, SAM for a right-hand circularly polarized beam with $\sigma = 1$. The instantaneous electric and magnetic field vectors are shown. **b**, IOAM in a vortex beam with $\ell = 2$. The instantaneous surface of a constant phase is shown. **c**, EOAM due to the propagation of the beam at a distance **R** from the coordinate origin.

and highly efficient spin-dependent shaping and control of light[48–55]. Combining SOI with structured materials provides a versatile platform for optical spin-based elements with desired functionalities[5,54–57].

(4) Any surface or waveguide mode possesses evanescent field tails. Coupling transversely propagating circularly polarized light to these evanescent tails results in a robust spin-controlled unidirectional excitation of the surface or waveguide modes[58–65]. This is a manifestation of the extraordinary transverse spin of evanescent waves[66,67] which can be associated with the quantum spin-Hall effect of light[68]. Because of its fundamental origin and robustness with respect to details of the system, this effect offers a link to topological photonics[69], quantum-optical networks[70], spin-controlled unidirectional interfaces and optical diodes[71].

In this Review we aim to provide a universal framework for the characterization of a variety of SOI phenomena. We explain various manifestations of SOI using the same underlying concepts: angular momenta and geometric phases. Such a unifying description provides a thorough understanding of SOI phenomena, explains the main features of their complex behaviour in various systems, and illuminates their fundamental origin.

Angular momenta and geometric phases

Two important fundamental concepts underpin the SOI of light: optical angular momenta[72–74] and geometric (Berry) phases[75,76]. These topics have been studied and reviewed extensively over the past two decades; here we only summarize the basic aspects that are crucial for understanding SOI phenomena.

Light carries momentum, which can be associated with its propagation direction and mean wavevector $\mathbf{P} = \langle\mathbf{k}\rangle$ (hereafter we consider dynamical quantities per photon in units of $\hbar = 1$). Structured light also carries different kinds of angular momentum (AM) (Box 1). For paraxial (collimated) optical beams, AM can be decomposed into three separately observable components: spin AM (SAM) **S**; intrinsic orbital AM (IOAM) $\mathbf{L}^{\text{int}}$; and extrinsic orbital AM (EOAM) $\mathbf{L}^{\text{ext}}$. These three types of optical AM can be associated with circular polarizations, optical vortices inside the beam, and beam trajectory, respectively. In addition to momentum, these three AM are determined by the following key parameters: helicity $\sigma = \pm1$, which corresponds to the right- and left-hand circular polarizations; vortex quantum number ℓ, which can take any integer value; and transverse coordinates of the beam centroid $\mathbf{R} = \langle\mathbf{r}\rangle$ (Box 1).

The interplay and mutual conversion between these three types of optical AM represent SOI of light. Namely, the interaction between SAM and EOAM results in a family of spin-Hall effects — the helicity-dependent position or momentum of light. In turn, the coupling between SAM and IOAM produces spin-to-orbital AM conversions — helicity-dependent optical vortices. Finally, the 'orbit–orbit coupling' between IOAM and EOAM[77,78] causes orbital-Hall effects, which are vortex-dependent shifts of optical beams. Orbital-Hall effects are similar to the spin-Hall effects considered here and are thus mostly left out of this Review.

Geometric phases underlie the spin-dependent deformations of optical fields (Box 2). These phases can be explained as originating from the coupling between SAM and coordinate frame rotations that are naturally determined in each particular problem. For example, rotating the transverse *xy* coordinates induces opposite phase shifts in the right- and left-hand circularly polarized waves propagating along the *z*-axis. Such helicity-dependent phases underpin the spin-dependent shaping of light via

NATURE PHOTONICS DOI: 10.1038/NPHOTON.2010.201

Box 2 | Geometric phases.

Geometric phases in optics originate from the coupling between intrinsic angular momentum and rotations of coordinates. Rotations of local coordinate frames with respect to the global laboratory frame enable convenient descriptions of optical problems that involve either curvilinear trajectories of light (rotating the frame with the trajectory) or media with spatially varying anisotropy (aligning the frame with the anisotropy axis). The simplest example of the effect of coordinate rotations on paraxial light is shown in panel **a**. Circularly polarized waves propagating in the z-direction and carrying SAM $\sigma\bar{\mathbf{z}}$ are characterized by the electric-field polarization vectors $\mathbf{E}^{\sigma} \propto \bar{\mathbf{x}} + i\sigma\bar{\mathbf{y}}$, where $\sigma = \pm 1$ and the overbars denote the unit vectors of the corresponding axes. Rotation of the coordinates by an angle $\varphi\bar{\mathbf{z}}$ (that is, about the z-axis) induces helicity-dependent phases $\mathbf{E}^{\sigma} \rightarrow \mathbf{E}^{\sigma}\exp(-i\sigma\varphi)$. This is the geometric phase $\Phi_{\mathrm{G}} = -\sigma\varphi$ given by the product between the SAM and the rotation angle.

This example allows a straightforward extension to the general case with arbitrary directions of propagation and rotation. If the wave carries SAM $\mathbf{S}$, and the coordinate frame experiences rotations with an angular velocity $\mathbf{\Omega}_{\zeta}$ (defined with respect to the parameter ζ, which can be a coordinate or time), then during this ζ-evolution the wave acquires a geometric phase $\Phi_{\mathrm{G}} = -\int \mathbf{S} \cdot \mathbf{\Omega}_{\zeta}\, \mathrm{d}\zeta$. This simple 'dynamical' form[7,34] unifies the so-called Pancharatnam–Berry and spin-redirection types of geometric phase[75,76], and also unveils its similarity with the rotational Doppler shift[138,139] and Coriolis effect[140,141].

An important example that underlies the SOI of light in isotropic media is the geometric phase caused by variations of the wavevector direction, $\bar{\mathbf{k}} = \mathbf{k}/k$, in nonparaxial fields. The polarization of a plane-wave in vacuum is always orthogonal to its wavevector, such that $\mathbf{k} \cdot \mathbf{E}(\mathbf{k}) = 0$. This transversality condition means that the polarization is dependent on the wavevector and is tangent to the $\bar{\mathbf{k}}$-sphere of directions in wavevector space (panel **b**). The geometric parallel transport of the polarization vector on the curved surface of this sphere reveals inevitable rotations between the transported vector and the global spherical coordinates, and, therefore, induces geometric phases in circularly polarized waves. Using the helicity basis of circular polarizations $\mathbf{E}^{\sigma}(\mathbf{k})$ attached to the spherical coordinates (θ, ϕ) in wavevector space, geometric-phase phenomena are described by the so-called Berry connection $\mathbf{A}^{\sigma}$ and Berry curvature $\mathbf{F}^{\sigma}$ (ref 4,7,8,75,76,79):

$$\mathbf{A}^{\sigma}(\mathbf{k}) = -i\mathbf{E}^{\sigma\star}\cdot(\nabla_{\mathbf{k}})\,\mathbf{E}^{\sigma} = -\frac{\sigma}{k}\cot\theta\,\bar{\boldsymbol{\phi}}, \quad \mathbf{F}^{\sigma}(\mathbf{k}) = \nabla_{\mathbf{k}} \times \mathbf{A}^{\sigma} = \sigma\frac{\mathbf{k}}{k^3}$$

Despite their geometrical origin, these unusual quantities act as an effective 'vector-potential' and 'magnetic field' in wavevector space, with the helicity σ playing the role of the 'charge'. The Berry connection and Berry curvature therefore determine intrinsic SOI phenomena, such as the spin-Hall effect.

The Berry connection allows us to compare the phases of circularly polarized waves propagating in different directions. Namely, variations of the wavevector along a contour C on the $\bar{\mathbf{k}}$-sphere bring about the geometric phase $\Phi_{\mathrm{G}} = \int_{C}\mathbf{A}^{\sigma}\cdot\mathrm{d}\mathbf{k}$ (an analogue of the Aharonov–Bohm phase for the 'vector-potential' $\mathbf{A}^{\sigma}$). In particular, traversing a contour of constant θ, such as that shown in panel **b**, the right- and left-hand circularly polarized waves acquire opposite geometric phases $\Phi_{\mathrm{G}} = -\sigma\phi\cos\theta$ (so the linear-polarization vector rotates by an angle $-\phi\cos\theta$). This exactly coincides with the 'SAM-rotation coupling' expression $-S_z\phi$. For the whole loop, subtracting the 2π rotation of the $\bar{\phi}$-coordinate, this yields the global phase $\Phi_{\mathrm{G0}} = 2\pi\sigma(1 - \cos\theta)$, which is determined by the solid angle enclosed by the contour[75,76].

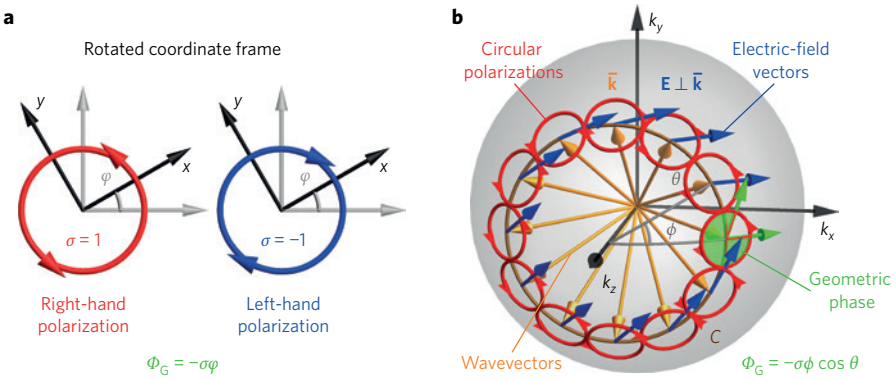

Rotation-induced geometric phases. a, A two-dimensional rotation of the transverse coordinates induces a helicity-dependent phase shift Φ_{G} in circularly polarized light. **b**, Three-dimensional variations in the wavevector direction involve non-trivial parallel transport of the electric-field vectors on the sphere of directions. Rotation of the transported vector with respect to spherical coordinates produces a helicity-dependent geometric phase difference Φ_{G} between circularly polarized waves propagating in different directions.

two-dimensional anisotropic structures with varying orientation of the anisotropy axis[5,6,48–50,52,53]. A more sophisticated example of the geometric phase, which is inherent in free-space Maxwell's equations, is related to three-dimensional variations in the direction of the wavevector $\mathbf{k}$ (and the SAM attached to it). Comparing the phases of circularly polarized waves propagating in different directions involves SO(3) rotations of coordinates and generates helicity-dependent geometric phases, which are described by the Berry connection and curvature on the sphere of directions in wavevector space[4,7,8,75,76,79] (Box 2). Such spin-redirection geometric phases underpin intrinsic SOI phenomena, which take place in isotropic inhomogeneous media[3,4,7,13–16,18–20] and nonparaxial free-space fields[4,8,23–26,28–37]. Note that the wavevector-dependent geometric phases occur for variations in individual wavevectors $\mathbf{k}$ in the Fourier spectrum of the field, as well as for the evolution of the mean wavevector $\langle\mathbf{k}\rangle$ (momentum) of the whole beam.

Spin-Hall effects in inhomogeneous media

The first important example of SOI occurs in the propagation of paraxial light in an inhomogeneous isotropic medium. It is well-known from geometrical optics that light changes its direction of propagation and momentum due to refraction or reflection at medium inhomogeneities. However, in traditional geometrical optics in the absence of anisotropy, the trajectory of an optical beam is independent of its polarization[80]. This is because geometrical optics neglects wavelength-scale phenomena, which become important for modern nano-optics. Going beyond the geometrical-optics approximation and considering wavelength-order corrections to the evolution of light introduces polarization-dependent perturbations of the light trajectory coming from the intrinsic SOI in Maxwell's equations[7].

Let us consider the propagation of light in a gradient-index medium with refractive index $n(\mathbf{r})$. The smooth trajectory of a light beam in such a medium can be described by mean coordinates $\mathbf{R}$ and momentum $\mathbf{P}$, which vary with the trajectory length τ. Considering 'semiclassical' (that is, wavelength-order) corrections to this 'mechanical' formalism, the trajectory of light in a gradient-index medium is described by the following equations of motion[3,7,13,14,18,81]:

$$\dot{\mathbf{P}} = \nabla n(\mathbf{R}), \quad \dot{\mathbf{R}} = \frac{\mathbf{P}}{P} - \frac{\sigma}{k_0}\frac{\mathbf{P}\times\dot{\mathbf{P}}}{P^3} \tag{1}$$

Here the overdot stands for the derivative with respect to τ, $k_0 = \omega/c$ is the vacuum wavenumber, and we use the dimensionless momentum $\mathbf{P} = \langle\mathbf{k}\rangle/k_0$. The last term in the second equation (1) describes the transverse spin-dependent displacement of the trajectory, that is, the spin-Hall effect of light (Fig. 1a). This effect was originally known as the optical Magnus effect[3]. Later, it was shown that the helicity-dependent term in equations (1) can be considered as a 'Lorentz force' produced by the Berry curvature $\mathbf{F}^{\sigma}(\mathbf{P})$ acting in momentum space[7,13,14,18] (Box 2). The Berry connection and curvature act as a geometry-induced 'vector-potential' and 'magnetic field' in momentum space, thereby revealing the geometrodynamical nature of the SOI of light. In doing so, the Berry connection underlies the evolution of the polarization along the curvilinear trajectory, which obeys the parallel-transport law and is described by the geometric phases $\Phi_G = \int \mathbf{A}^{\sigma}(\mathbf{P})\cdot d\mathbf{P}$ for the two helicity components (Fig. 1a)[7,75,76]. The measurement of this polarization evolution in coiled optical fibres was one of the first observations of the Berry phase[82,83].

The spin-Hall effect and the equations of motion for spinning light (equations (1)) are completely analogous to those for electrons in condensed-matter[84] and high-energy[10] systems. Whereas the electron's momentum is driven by an applied electric field, in optics the refractive-index gradient plays the role of the external driving force. Strikingly, the spin-Hall effect shows that an isotropic inhomogeneous medium exhibits circular birefringence. However, in contrast with anisotropic media, this birefringence is determined solely by the intrinsic properties of light, namely, by its SAM. Moreover, the helicity-dependent shift of the trajectory is intimately related to the conservation of the total AM of light. Indeed, for spherically-symmetric profiles $n(\mathbf{r})$, equations (1) possess the corresponding integral of motion[14]:

$$\mathbf{J} = \mathbf{R}\times\mathbf{P} + \sigma\mathbf{P}/P = \mathbf{L}^{\mathrm{ext}} + \mathbf{S} = \text{constant}$$

Figure 1a,b shows an example of the spin-Hall effect measured for the helical trajectory of light inside a glass cylinder[18]. A distance of several wavelengths between the positions of the right- and left-handed circularly polarized beams ($\sigma = \pm 1$) was achieved due to the accumulation of the effect along several coils of the trajectory. This experimental observation is of fundamental importance for the physics of relativistic spinning particles[10,81]. Indeed, direct measurements of analogous spin-dependent electron trajectories are far beyond the current experimental capabilities, and only indirect measurements of the spin-Hall effect are possible in condensed-matter physics[85].

Equations (1) describe a 'macroscopic' picture of the spin-Hall effect, which contains only the mean beam parameters. What causes this unusual effect at the 'microscopic' level of the individual plane-waves that form the beam? This can be understood by considering another example of the spin-Hall effect.

Instead of a gradient-index medium, we now consider the refraction or reflection of a paraxial beam at a sharp interface between two isotropic media. This problem is described by Snell's law and the Fresnel equations[1]. However, these equations are valid for a single plane-wave impinging at the interface. At the same time, a finite-size beam comprises multiple plane-waves with slightly different wavevectors $\mathbf{k}$ (Fig. 1c), which gives them slightly different planes of incidence entering the Fresnel reflection/refraction equations. Let the z-axis be directed along the normal to the interface, and the incident-beam momentum lie in the xz plane with a polar angle of incidence θ, such that $\langle k_y\rangle = 0$. The planes of incidence for individual plane-waves in the beam are then rotated by the azimuthal angle $\phi = \bar{k}_y/\sin\theta$ about the z-axis (Fig. 1c) and, hence, induce geometric phases $\Phi_G(k_y) = S_z\phi = \sigma\bar{k}_y\cot\theta$ for the circularly polarized waves (Box 2)[16,19,86]. The k_y-gradient of this geometric phase determines a typical beam shift along the y-axis, that is, out of the plane of incidence. Taking into account the Fresnel coefficients of the interface and similar geometric phases for the reflected/refracted beams, one can obtain accurate equations for the spin-dependent shifts of these beams[15,17,19,86]. In the simplest case of total reflection from the interface, the reflected beam acquires the following helicity-dependent shift with respect to the incident beam:

$$Y' = -\frac{\sigma+\sigma'}{k}\cot\theta \tag{2}$$

where σ' and Y' are the helicity and centroid position of the reflected beam (setting $Y = 0$ for the incident beam).

The transverse shift (equation (2)) is known as the Imbert–Fedorov shift, which was predicted and observed a long time ago for the total internal reflection of light[87,88]. However, studies of the Imbert–Fedorov effect were full of controversies. It was only recently that correct theoretical calculations[15,86] and definitive measurements[16] elucidated its nature as a SOI effect. (Note the close similarity between equation (2) and the Berry connection in Box 2 (ref. 14).) Figure 1d shows measurements[16] of the spin-Hall effect splitting between the right- and left-hand circularly polarized components in a linearly polarized beam refracted at an air–glass interface. Extraordinary angstrom accuracy was achieved by using the 'quantum weak measurements' technique with near-orthogonal input and output polarizers[16,20,89,90].

Akin to equation (1), the spin-Hall shift (equation (2)) is intimately related to the interplay between the SAM and EOAM of the beams induced at the interface[15,86,91,92]. Namely, this shift ensures the conservation of the z-component of the total AM between the incident and reflected beams, such that $S_z = S_z' + L_z^{\mathrm{ext}\prime}$, where $S_z = \sigma\cos\theta$, $S_z' = -\sigma'\cos\theta$ and $L_z^{\mathrm{ext}\prime} = -Y'k\sin\theta$. Interestingly, the SOI of light at sharp interfaces also causes transverse polarization-dependent deflections (that is, momentum shifts P_y') of the reflected or refracted beams[17,19,86,93]. Figure 1e shows the spin-Hall effect and images of the polarization-dependent coordinate and momentum shifts generated at the 'refraction' of the incident beam of light into the surface plasmon–polariton beams propagating along a metal

NATURE PHOTONICS DOI: 10.1038/NPHOTON.2010.201

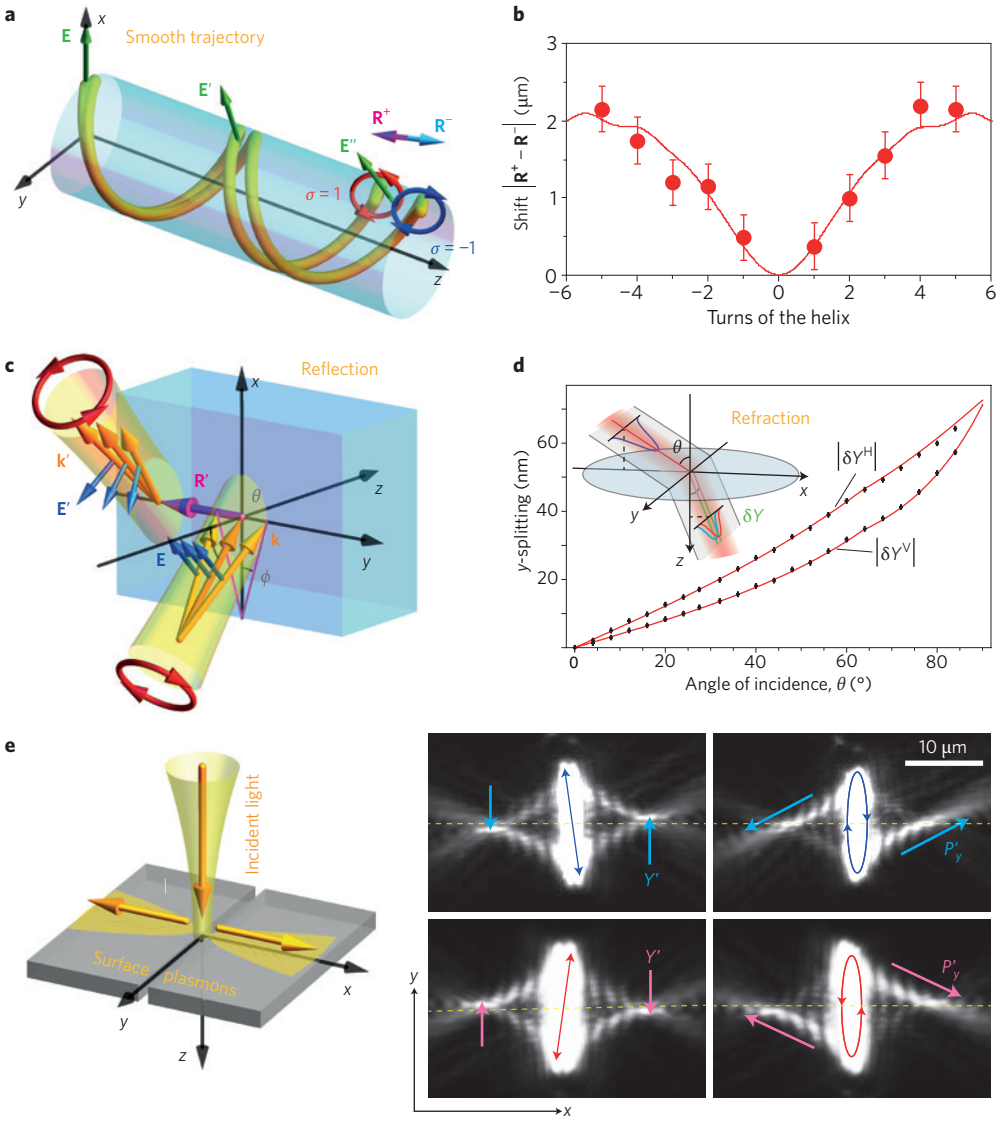

Figure 1 | Spin-Hall effects for paraxial beams in inhomogeneous media. a, Propagation of light along a curvilinear trajectory causes a transverse spin-dependent deflection produced by a 'Lorentz force' from the Berry curvature. This is the spin-Hall effect of light (equations (1)). In turn, the linear-polarization vector obeys the parallel-transport law along the trajectory due to the geometric phase difference between opposite circular polarizations. **b**, Measurements of this spin-Hall effect for a helical light trajectory shown in **a**. **c**, Similarly to **a**, a spin-dependent transverse shift (equation (2)) occurs in beam reflection or refraction at a planar interface. The spin-Hall effect is produced by k_y-dependent geometric phases acquired by different plane-waves in the beam spectrum, which propagate in different planes (marked by the azimuthal angles ϕ). The spin-Hall shift generates EOAM (Box 1, panel **c**) and provides AM conservation in the system. **d**, Precision 'quantum weak measurements' of the spin-Hall splitting in a linearly polarized beam refracted at an air–glass interface. **e**, Observation of the spin-Hall shifts in both coordinate and momentum using the weak-measurement approach and 'refraction' of the z-propagating light into the x-propagating surface plasmon-polariton beams. The polarizations of the incident light are shown by the red and blue double-arrows in the right-hand panels. Figure reproduced with permission from: **b**, ref. 18, Nature Publishing Group; **d**, ref. 16, AAAS; **e** (right), ref. 20, APS.

film[20]. Typical subwavelength shifts are amplified to the beam-width scale using 'quantum weak measurements'[16,89,90].

Spin-Hall effects are ubiquitous at any optical interface. They have been measured at interfaces with metals[94], uniaxial crystals[95] and semiconductors[96], as well as nanometal films[21], graphene layers[22] and metasurfaces[97]. The spin-Hall shifts exhibit an interesting anomaly near the Brewster angle[15,90,98,99] and a fine interplay with the Goos–Hänschen (in-plane) shifts[17,19,89,90,100]. Because every optical device and component operates with finite-size beams and not plane-waves, the spin-Hall effects are always present at optical interfaces and inevitably affect the field distribution on the wavelength scale. On the one hand, they must be taken into account as inevitable SOI-induced aberrations. On the other hand, 'quantum weak measurement' amplification and the dependence of the spin-Hall shifts on the material parameters allow the spin-Hall effect to be used for precision metrology[21,22].

Optical spin-Hall effects originate from the interaction between SAM and EOAM, leading to mutual interplay between the polarization and trajectory of light. A quite similar interaction between IOAM and EOAM (vortex and trajectory) occurs for vortex beams in inhomogeneous media[19,78,101–106]. In this case, beams experience ℓ-dependent transverse shifts at the medium inhomogeneities. These can be regarded as the 'orbital-Hall effect' and 'orbit–orbit interactions' of light.

SOI in nonparaxial fields

The above examples of the spin-Hall effect in isotropic media are based on intrinsic SOI properties that require variations of wavevectors in the beam spectrum. This hints that SOI may naturally be enhanced in nonparaxial fields: for example, beams tightly focused by high-numerical-aperture lenses or scattered by small particles (Fig. 2a,d). Under such circumstances, the fields become inhomogeneous at the wavelength scale, and SOI effects can strongly affect the field distributions.

Remarkably, SOI manifest even in free-space nonparaxial light. Consider, for example, focused circularly polarized vortex beams carrying spin and IOAM. The simple association of SAM and IOAM with the polarization helicity and vortex (applicable for paraxial beams in Box 1), respectively, is no longer valid. For nonparaxial beams, which consist of circularly polarized plane-waves (helicity $\sigma = \pm 1$) with wavevectors forming a cone at an angle θ (like in Box 2, panel **b**), the SAM and IOAM become[8,31,38,107,108]:

$$\mathbf{S} = \sigma \cos\theta \frac{\mathbf{P}}{P}, \quad \mathbf{L} = [\ell + \sigma(1 - \cos\theta)] \frac{\mathbf{P}}{P} \tag{3}$$

The total intrinsic AM of the beam is preserved, giving $J_z = S_z + L_z = \sigma + \ell$ (we assume z-propagating beams), which means equations (3) can be interpreted as if part of the SAM was transferred to the IOAM. This is another fundamental manifestation of SOI: the spin-to-orbital AM conversion. Part of the orbital AM becomes helicity-dependent; that is, a helicity-dependent vortex should appear even in beams with $\ell = 0$ (Fig. 2b)[25–28,31,109]. Importantly, this effect is closely related to the geometric phase between the azimuthally distributed wavevectors $\mathbf{k}$ in the beam spectrum (Box 2, panel **b**)[8,31]. Using the global geometric phase Φ_{G0} between these wavevectors (Box 2), the converted part of the AM can be written as $\Delta L_z = -\Delta S_z = \Phi_{G0}/2\pi$. For the largest aperture angle $\theta = \pi/2$, $\Phi_{G0} = 2\pi$ and the conversion efficiency reaches 100%; that is, all the paraxial SAM is transferred to the IOAM[29].

To understand the origin of the spin-to-orbital AM conversion, note that focusing with a high-numerical-aperture lens rotates the wavevector of the incoming collimated beam in the meridional planes and thus generates a conical $\mathbf{k}$-distribution in the focused field (Fig. 2a). This is accompanied by rotations of the local polarization vectors $\mathbf{E}$, which are attached and orthogonal to each $\mathbf{k}$. Notably, this polarization evolution (described by the Debye–Wolf approach[110]) represents parallel transport on the $\bar{\mathbf{k}}$-sphere of directions (Box 2, panel **b**) from the north pole $\theta = 0$ (incoming light $\mathbf{E}$) to $\theta \neq 0$ (focused field $\mathbf{E}'$). In the global basis of the circular ($\bar{\mathbf{x}} + i\sigma\bar{\mathbf{y}}$)-polarizations and longitudinal $\bar{\mathbf{z}}$-component, this three-dimensional rotational transformation of the electric field is described by the following unitary matrix[31]:

$$\mathbf{E}' = \begin{pmatrix} a & be^{-2i\phi} & \sqrt{2ab}\, e^{-i\phi} \\ -be^{2i\phi} & a & \sqrt{2ab}\, e^{i\phi} \\ -\sqrt{2ab}\, e^{i\phi} & -\sqrt{2ab}\, e^{-i\phi} & a - b \end{pmatrix} \mathbf{E} \tag{4}$$

where $a = \cos^2(\theta/2)$ and $b = \sin^2(\theta/2)$. In equation (4), the off-diagonal elements contain the azimuthal vortex factors and are responsible for the AM conversion. Owing to the presence of these elements, the incoming circularly polarized light with helicity σ acquires an oppositely polarized component with helicity $-\sigma$ and vortex factor $b\exp(2i\sigma\phi)$, as well as a longitudinal z-component with vortex factor $\sqrt{(2ab)}\exp(i\sigma\phi)$. For small numerical apertures, the longitudinal component plays the leading role in the AM conversion. These helicity-dependent vortex components produce the helicity-dependent IOAM (equations (3)) in the focused field (Fig. 2a)[8,28,31,109].

The presence of helicity-dependent vortices and IOAM in focused light was observed using probe particles that interact with the focal field[25,26,109] (Fig. 2b). The particles experienced transverse orbital rotation around the beam axis (which is characteristic of optical vortices in the dipole-coupling approximation[74,111–113]), with the sense of rotation determined by the helicity of the incoming wave, which had no vorticity prior to focusing. Such mechanical manifestations of the SOI can play an important role in optofluidics and optical manipulations using nonparaxial light.[39]

Notably, the above AM conversion immediately reveals itself in the helicity-dependent intensity distributions of the focused fields. Namely, the mean radius of a focused vortex beam is determined by its σ-dependent IOAM value $R \sim |L_z|/k\sin\theta$ (refs 8,31). Due to this effect, a beam with anti-parallel SAM and IOAM becomes more strongly focused than a similar beam with parallel SAM and IOAM. The most striking manifestation of this effect appears for vortex beams with $|\ell| = 1$ (Fig. 2c). According to the transformation (equation (4)), the z-component of the field has a vortex charge $\ell + \sigma$. Therefore, for $\ell\sigma = 1$ this component represents a charge-2σ vortex with vanishing intensity in the beam centre, whereas for $\ell\sigma = -1$ this is a charge-0 vortex with maximum intensity in the centre. This helicity-dependent switching of the central intensity was observed in experiments[23,29] and employed for spin-controlled transmission of light via chiral nano-apertures[42] and AM-induced circular dichroism in non-chiral structures[114].

The SAM–IOAM coupling in nonparaxial optical fields is largely independent of how the field was generated. Instead of high-numerical-aperture focusing, one can consider dipole Rayleigh scattering by a small particle, which generates a similar conical distribution of the outgoing wavevectors (Fig. 2d). The electric-field transformation in dipole scattering to the far-field direction $\bar{\mathbf{k}} = \bar{\mathbf{r}}$ is given by[1] $\mathbf{E}' \propto -\bar{\mathbf{r}} \times (\bar{\mathbf{r}} \times \mathbf{E})$, which can be written in a matrix form very similar to equation (4)[31]. Therefore, the spin-to-orbital AM conversion also appears in the scattering of circularly polarized light[24,30,31,43,115,116].

Because focusing and scattering both produce strong SOI, these phenomena play an important role in high-resolution optical microscopy and the imaging of scattering processes[35,40]. This can be seen in the Stokes polarimetry of the paraxial field at the output of the imaging system. The superposition of the original σ-polarized state and the converted ($-\sigma$)-polarized state with the $\exp(2i\sigma\phi)$ vortex generates characteristic 'four-petal' patterns in the first and second Stokes parameters Σ_1 and Σ_2 (Fig. 2e). This effect was observed in systems of different nature and scales: diffusive backscattering from microparticle suspensions[40,41,117], scattering by liquid-crystal droplets[51] and dipole nanoparticle scattering[35]. Another interesting example of spin-to-orbital AM conversion occurs in the reflection of circularly polarized light from a conical mirror[118].

Spin-to-orbital AM conversion can be interpreted as being an azimuthal spin-Hall effect in cylindrically symmetric fields[28,30,119]. Breaking this cylindircal symmetry results in a pronounced spin-Hall effect in the direction orthogonal to the symmetry-breaking axis[8,32–37]. For example, illuminating only the $x > 0$ half of a high-numerical-aperture lens results in a subwavelength transverse shift of the focal spot[8,32–34], giving $Y' \propto \sigma/k$. Moreover, a high-numerical-aperture microscope with a dipole-scatterer specimen allows a dramatic inversion of the spin-Hall effect scale[35]. Instead of subwavelength shifts caused by helicity switching (Fig. 1), subwavelength x-displacements of the particle cause a giant macroscopic y-redistribution of the SAM density (that is, the third Stokes parameter Σ_3) in the exit pupil (Fig. 2f). An analogous 'orbital-Hall effect' — the ℓ-dependent transverse redistribution of intensity — can be seen in the asymmetric scattering of vortex beams[120].

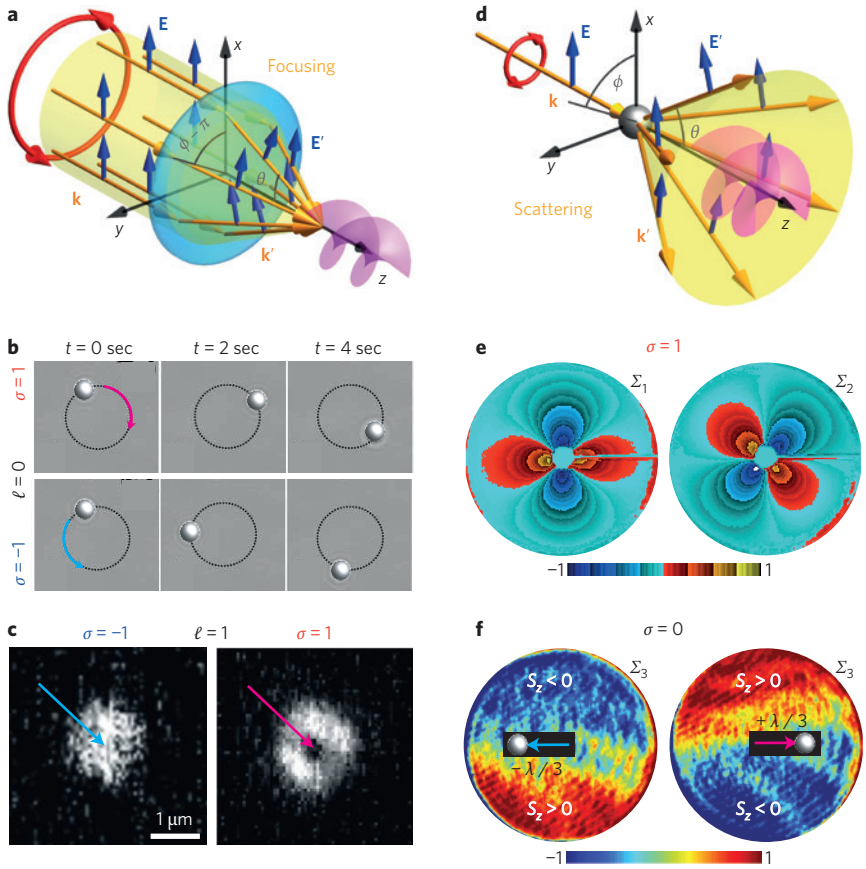

Figure 2 | SOI in nonparaxial light. a, Tight focusing of a paraxial wave generates a conical wavevector distribution (cf. Box 2, panel **b**). The resulting 3D field has components with helicity-dependent vortices (that is, intrinsic orbital AM). This is the spin-to-orbital AM conversion, given by equations (3) and (4). **b**, Experimental observation of the helicity-dependent vortex and orbital AM in a focused field via the helicity-dependent orbital motion of a probe particle. **c**, Manifestation of the spin-to-orbital AM conversion in the helicity-dependent intensity of the focused field. Tightly focused beams with $\ell\sigma = 1$ and $\ell\sigma = -1$ have zero and maximum intensity in the centre, respectively. **d**, Rayleigh scattering by a small dipole particle produces a spherical redistribution of the field and the AM conversion, similar to the focusing case. **e**, The spin-to-orbital AM conversion is clearly seen in the imaging and polarimetry of scattering processes as 'four-petal' patterns in the Stokes parameters Σ_1 and Σ_2. Here, experimental figures for the diffusion-backscattering of light from a particle suspension are shown. **f**, Giant spin-Hall effect induced by the breaking of cylindrical symmetry in the system. Subwavelength x-displacements of a Rayleigh nanoparticle in a high-numerical-aperture imaging system produce a macroscopic y-separation of the spin AM density (the third Stokes parameter Σ_3) in the linearly polarized light. Panels **b**, **c**, **e** and **f** correspond to the transverse xy-plane distributions. Figure reproduced with permission from: **b**, ref. 109, OSA; **c**, ref. 23, OSA; **e**, ref. 40, OSA; **f**, ref. 35, APS.

These examples show that SOI crucially affect the field distributions and properties of every instance of nonparaxial light, including fields that interact with subwavelength structures. As such, SOI phenomena inevitably emerge in numerous nano-optical, plasmonic and metamaterial systems, which crucially involve subwavelength scales and structures[121].

SOI produced by anisotropic structures

Until now we have considered only 'intrinsic' SOI effects, which originate from the fundamental properties of Maxwell's equations. Such SOI phenomena are quite robust with respect to perturbations and the specific details of locally isotropic media. Another class of SOI effects can be induced by particular properties of the medium. These 'extrinsic' effects emerge in anisotropic media and structures, including metamaterials, and thus can be designed to achieve various functionalities. Combining anisotropy and inhomogeneities allows efficient control of the polarization degrees of freedom, as well as controllable shaping of the intensity and phase distributions. In such media, strong SOI can be achieved even with paraxial z-propagating light interacting with xy planar structures. In this case, varying the orientation of anisotropic scatterers produces simple two-dimensional geometric phases (Box 2, panel **a**), leading to SOI.

Let us consider paraxial light transmission through a planar anisotropic element (Fig. 3a). For simplicity, we assume a transparent retarder that provides a phase shift δ between the orthogonal linear polarizations, with the anisotropy axis oriented at an angle α in the xy plane. Considering the problem in the local coordinates attached to the anisotropy axis, the evolution of light is described by the transmission Jones matrix $T = \mathrm{diag}(e^{i\delta/2}, e^{-i\delta/2})$. Performing a rotation by the angle α to the laboratory coordinate frame, and also writing this matrix in the helicity basis of right- and left-hand circular polarizations, the Jones-matrix transformation of the wave polarization becomes[5,6,48–50,122]

$$\mathbf{E}' = \begin{pmatrix} \cos\dfrac{\delta}{2} & i\sin\dfrac{\delta}{2}e^{-2i\alpha} \\ i\sin\dfrac{\delta}{2}e^{2i\alpha} & \cos\dfrac{\delta}{2} \end{pmatrix} \mathbf{E} \qquad (5)$$

Here the off-diagonal elements with phase factors $\exp(\mp 2i\alpha)$ originate from geometric phases induced by the rotation of coordinates (Box 2, panel **a**). For the half-wave retardation $\delta = \pi$, the matrix (equation (5)) becomes off-diagonal and describes the transformation of the $\sigma = \pm 1$ circularly polarized light into the opposite polarization $\sigma' = \mp 1$, with the geometric phase difference $\Phi_G = 2\sigma\alpha$. This geometric phase is usually derived using the Pancharatnam–Berry formalism on the Poincaré sphere[5,6,48–50], but here we use the much simpler considerations shown in Box 2.

The off-diagonal geometric-phase elements of equation (5) allow the helicity-dependent manipulation of light using the orientation of the anisotropy axis. In particular, anisotropic subwavelength gratings with a space-variant orientation $\alpha = \alpha(x, y)$ have been employed for the geometric-phase-induced shaping of light[5,48,49,52,122–125]. Moreover, liquid-crystal films and droplets represent natural tunable optical elements with spatially varying anisotropy, which are capable of spin-controlled shaping of light[6,50,51,126,127]. The two most important cases of such planar SOI elements are shown in Fig. 3b,c.

Let the orientation of the anisotropy axis change linearly with one of the coordinates, such that $\alpha = \alpha_0 + qx$ (Fig. 3b). In this case, for a half-wave retardation, the σ-polarized light is converted into light of opposite helicity and also acquires the helicity-dependent geometric-phase gradient $\Phi_G = 2\sigma qx$. This phase gradient produces a transverse helicity-dependent component in the momentum (wavevector) of light, giving $P_x' = 2\sigma q$. Thus, the x-variant anisotropic structure deflects right- and left-hand polarized beams in opposite x-directions[5,48,53,122]. This can be considered as the anisotropy-induced spin-Hall effect of light. Whereas in the intrinsic spin-Hall effect (Fig. 1) the coordinate shift is caused by the wavevector gradient of the 'three-dimensional' geometric phase (Box 2, panel **b**), here the momentum shift is generated by the coordinate gradient of the 'two-dimensional' geometric phase (Box 2, panel **a**). This extrinsic spin-Hall effect generated by the space-variant anisotropic elements allows complete spatial separation of the two spin states of light: a linearly polarized light with $\sigma = 0$ is transformed into two well-split $\sigma' = \pm 1$ beams propagating in different directions (Fig. 3b)[48]. Therefore, such anisotropic inhomogeneous structures offer efficient polarization beam splitters and spin-based optical switches[5,122]. Moreover, if the transmitted beam is converted into x-propagating surface-plasmon waves, then the two spin components propagate in opposite directions[53]. This provides a helicity-controlled directional coupler that can be implemented across a variety of photonic platforms.

Assume now that the anisotropy-axis orientation varies linearly with the azimuthal coordinate φ in the xy plane, $\alpha = \alpha_0 + q\varphi$ (Fig. 3c). Here $q = 0, \pm 1/2, \pm 1, \ldots$, and the structure has a direction singularity at the coordinate origin. In this case, the anisotropic half-waveplate reverses the helicity and generates an azimuthal geometric-phase difference between the transmitted and incident fields, given by $\Phi_G = 2\sigma q\varphi$. This means that the transmitted beam becomes a vortex beam with topological charge $\ell' = 2\sigma q$ (refs 5,6,49,50,124). In other words, a spin-to-orbital AM conversion takes place. Such azimuthal anisotropic structures (also called q-plates) offer efficient spin-controlled converters and generators of optical vortex beams carrying IOAM[5,6,49,50]. Note that the $q = 1$ anisotropic plate is rotationally symmetric with respect to the z-axis (Fig. 3c). In this case, the z-component of the total AM is conserved, such that $\sigma = \sigma' + \ell'$, and the Jones matrix (equation (5)) resembles the transverse xy sector of the nonparaxial focusing matrix (equation (4)). Very similar conversions of SAM into IOAM with $\ell' = 2\sigma$ occur in all cylindrically symmetric systems with effective anisotropy between the radial and azimuthal polarizations. Examples of this include the propagation of light along the optical axis of a uniaxial crystal[45,46,128], in cylindrical optical fibres[44], and focusing and scattering in rotationally symmetric systems with paraxial input and output[35,51]. In the generic case of $q \neq 1$, the rotational symmetry is absent, there is no AM conservation for light, and part of the optical AM is transferred to the medium[129,130].

The above examples demonstrate that inhomogeneous anisotropic planar structures provide a highly efficient tool for the spin-dependent shaping and control of light. Recently there has been enormous interest in the study of such structures, which can be considered as planar metamaterials (that is, metasurfaces)[56]. In the above examples, we essentially discussed two-scale structures with subwavelength gratings that provide local anisotropy and inhomogeneity larger than the wavelength (but smaller than the beam size). If the typical scales of the structure are comparable to the wavelength, these inhomogeneities can considerably modify the eigenmodes and spectral properties of light. Such structures can couple light to surface plasmon–polaritons and control the properties of these surface waves. In particular, chiral structures can generate a spin-dependent plasmonic distribution with vortices[29,131,132], and periodic crystal-like structures with broken spatial-inversion symmetry result in spin-dependent spectra of photonic quasiparticles[54,55,65,133]. The latter case is entirely analogous to the spin-dependent splitting of electron energy levels in solids with SOI[11,12]. Figure 3d shows an example[55] of such a plasmonic metasurface, together with the experimentally measured spin-polarized dispersion. The different spin states of the incident light are coupled to different propagation directions of surface plasmon-polaritons, depending on the frequency and orientation of the plasmonic crystal. Thus, the SOI of light at metasurfaces paves the avenue to spin-controlled photonics as an optical analogue of solid-state spintronics. Note that plasmonic resonances in nanostructures can produce additional polarization-dependent phases in the scattered light, which must be taken into account alongside the geometric phases.

Spin-direction locking via evanescent waves

After discussing artificial structures, we now return to the fundamental intrinsic properties of light. Recently, several experiments and numerical simulations have demonstrated remarkable spin-controlled unidirectional coupling between circularly polarized incident light and transversely propagating surface or waveguide modes[58–64,71,134–136] (Fig. 4b,c). In contrast with spin-directional coupling at metasurfaces (Fig. 3d,e), most of the above experiments have involved the use of planar interfaces without any structures. Moreover, the effect is incredibly robust to the details of the system and appears with near-100% polarization directionality at metal surfaces[58,59,61], nanofibres[60,62,71] and various waveguides[63,64,134–136]. This unique transverse spin-direction coupling originates from the fundamental spin properties of evanescent modes in Maxwell's equations.

So far we have discussed the fundamental AM and SOI properties of propagating waves (Box 1). Although some SOI effects have been demonstrated in plasmonic systems (for example, Fig. 1e), they merely mimicked the properties of propagating waves. However, evanescent waves are able to exhibit their unique AM properties. Namely, it was recently discovered that evanescent waves carry extraordinary transverse spin AM[66,67,74], which is in sharp contrast with prior knowledge regarding photon spin.

An evanescent wave, propagating along the z-axis and decaying in the x-direction, can be regarded as a plane-wave with complex wavevector $\mathbf{k} = k_z\bar{\mathbf{z}} + i\kappa\bar{\mathbf{x}}$ (Fig. 4a). Here, $k_z > k$ and κ is the decay constant. Importantly, owing to the transversality condition $\mathbf{E} \cdot \mathbf{k} = 0$, which underpins all the intrinsic SOI effects in optics, the evanescent-wave polarization acquires a longitudinal 'imaginary' (that is, phase-shifted by $\pi/2$) component, such that $E_z = -i(\kappa/k_z)E_x$. This means that the electric field of a linearly x-polarized wave rotates in

NATURE PHOTONICS DOI: 10.1038/NPHOTON.2010.201

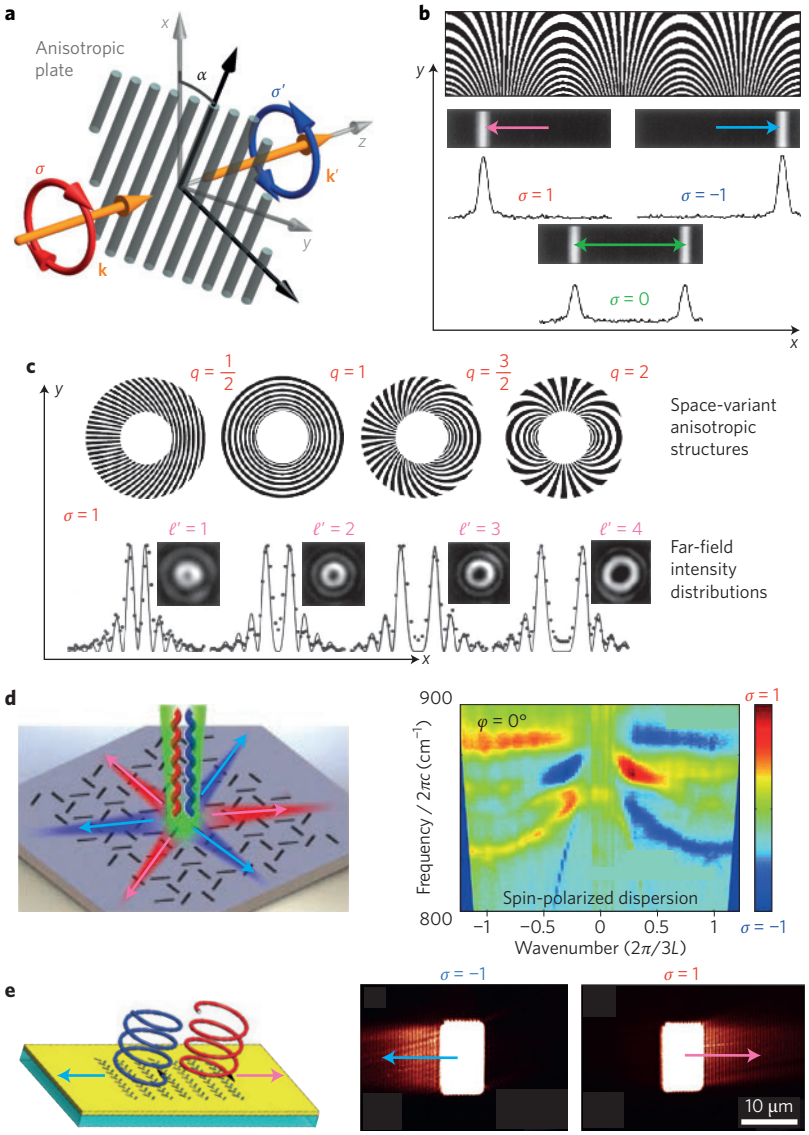

Figure 3 | SOI induced by planar anisotropic and inhomogeneous structures. a, Schematics of light transmission through a locally anisotropic subwavelength structure with the α-oriented anisotropy axis. **b**, The orientation of the anisotropy axis, α, is linearly varying with x, which induces a helicity-dependent geometric-phase gradient and transverse momentum of the transmitted light. Similarly to the spin-Hall effect, this deflects the two spin states of light ($\sigma = \pm 1$) in opposite directions and splits the linearly polarized light ($\sigma = 0$) into two spin components. **c**, The azimuthally-varying orientation $\alpha = q\varphi$ induces helicity-dependent geometric-phase vortices in the transmitted field. This allows for spin-to-orbital AM conversion and the spin-controlled generation of optical vortex beams. **d**, A periodic plasmonic structure with broken inversion symmetry provides a two-dimensional metamaterial with spin-dependent dispersion (see the thermal-emission dispersion in the right panel), analogous to that of electrons in solids with SOI. c is the speed of light and L is the nearest-antenna distance in the lattice. **e**, Another type of inversion-asymmetric structure, which provides controllable spin-direction coupling between light and surface plasmons. Figure reproduced with permission from: **b**, ref. 48, OSA; **c**, ref. 49, OSA; **d** (left), ref. 142, OSA; **d** (right), ref. 55, AAAS; **e**, ref. 54, AAAS.

the propagation xz plane, and thereby generates SAM directed along the orthogonal y-axis (Fig. 4a). Taking into account both electric- and magnetic-field contributions, it turns out that the transverse spin is independent of the polarization parameters and can be written in a universal vector form[67,68,74]:

$$\mathbf{S}_{\perp} = \frac{\mathrm{Re}\,\mathbf{k} \times \mathrm{Im}\,\mathbf{k}}{(\mathrm{Re}\,\mathbf{k})^2} \qquad (6)$$

The transverse SAM (equation (6)) represents a completely novel type of optical AM[74] that is in sharp contrast with the usual longitudinal SAM of light (Box 1). Strikingly, it is orthogonal to the wavevector and independent of the polarization. In particular, the transverse SAM is unrelated to the helicity of light, which is determined by the xy polarization components and is associated with the longitudinal z-directed SAM. The transverse spin in evanescent waves can be regarded as a distinct manifestation of the SOI of light, which is unrelated to geometric phases and originates directly from the transversality condition. Note that analogous transverse SAM can also appear locally in nonparaxial propagating fields[74].

Most importantly for applications, the direction of the transverse SAM (equation (6)) becomes uniquely locked with the direction of propagation of the evanescent wave. Oppositely propagating waves with $k_z > 0$ and $k_z < 0$ carry opposite transverse spins $S_y > 0$ and $S_y < 0$, respectively. It is this remarkable feature that is employed in spin-directional coupling using evanescent waves[58–64,71,134–136] (Fig. 4b,c). Indeed, in all systems[58–64,71,134–136] the

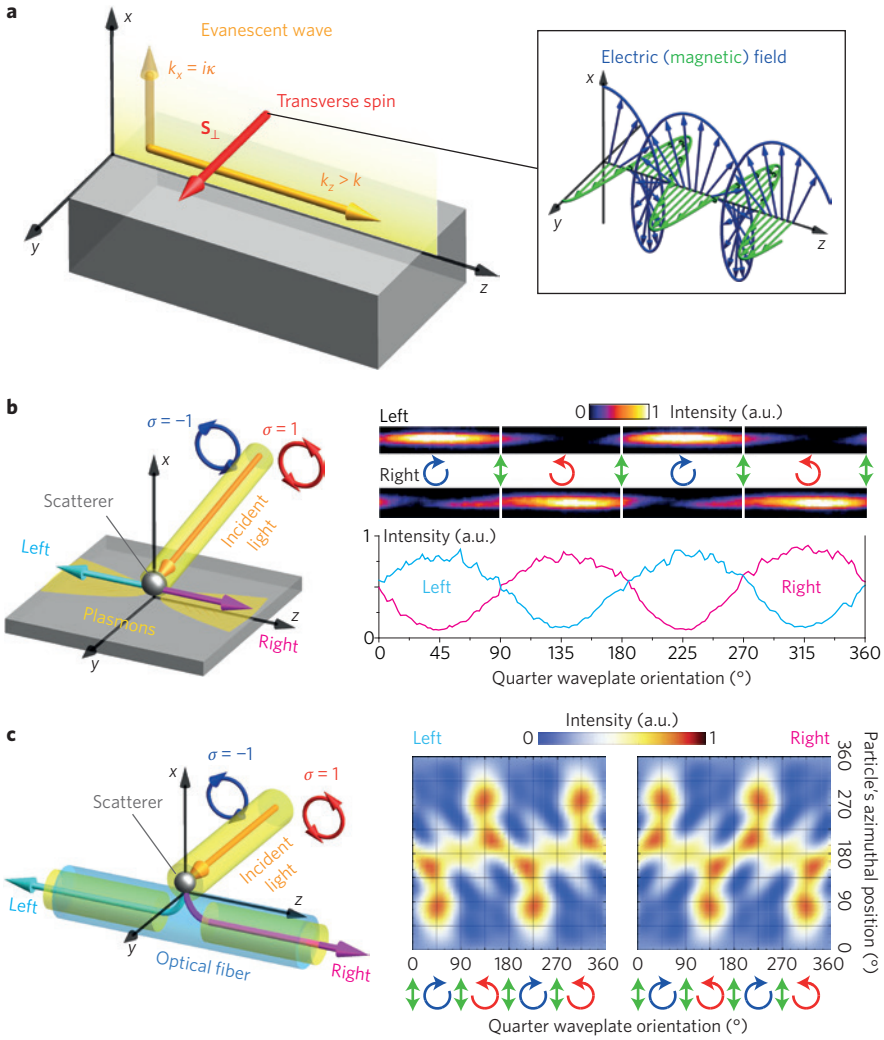

Figure 4 | Transverse spin in evanescent waves and spin-directional interfaces. a, A single evanescent wave propagating along the $x = 0$ interface in the z-direction and decaying in the $x > 0$ half-space. The complex wavevector $\mathbf{k}$ and the transversality condition together generate a xz plane rotation of the wave field (shown in the inset for the linearly x-polarized wave) and a transverse y-directed spin AM $\mathbf{S}_\perp$ (equation (6)). The sign of this spin depends on the propagation direction of the wave. **b**, Spin-controlled unidirectional coupling of the y-propagating light to the z-propagating surface plasmon-polaritons. The spin AM of the incident field matches the transverse spin of the surface plasmon and determines its direction of propagation. The right panel shows the measured intensities of the left- and right-propagating surface plasmon-polaritons as functions of the incident-beam polarization. **c**, An analogous transverse spin-direction coupling occurs for the z-propagating modes of an optical fibre. These modes are coupled to the y-propagating light via the evanescent tails of guided modes similar to surface plasmons in **b**. The right panel shows the guided light intensities at the left and right ends of the fiber as functions of the incident light polarization and azimuthal position of the scatterer with respect to the cylindrical fiber. Figure reproduced with permission from: **b** (right), ref. 61, Nature Publishing Group; **c** (right), ref. 60, AAAS.

incident light propagates along the transverse y-axis and carries the usual SAM that depends on its helicity, $S_y^{\mathrm{inc}} \propto \sigma$. This incident light is then coupled via some scatterer (a nanoparticle, atom or quantum dot) to evanescent x-decaying tails of the z-propagating surface or waveguide modes. Assuming that the SAM of the incident light matches the transverse SAM in the evanescent wave, $S_y^{\mathrm{evan}} \propto \mathrm{sgn}\, k_z$, the propagation direction of the mode with evanescent tails is determined by the helicity of the incident light, $\mathrm{sgn}\, k_z = \sigma$.

Figure 4b,c shows two examples of such spin-directional coupling to surface plasmon–polaritons[61] and nanofibre[60] modes. This effect has a remarkable near-100% polarization directionality and robustness with respect to the details of the system. It works with any interface that supports evanescent-tail modes and offers unique opportunities to be used in spin-chiral networks, spin-controlled gates, optical diodes[71] and other quantum-optical devices[70].

Remarkably, the universal character of spin-direction locking in evanescent waves can be associated with the quantum spin-Hall effect of photons[68], which makes it an optical counterpart of the quantum spin-Hall effect of electrons in topological insulators[137].

Concluding remarks

We have shown that the SOI of light originate from the fundamental properties of electromagnetic Maxwell waves and are thus inherent to all basic optical processes. Like relativistic SOI for electrons, optical SOI effects are typically small in geometrical-optics processes that deal with scales and structures much larger than the wavelength of light. However, at the subwavelength scales of modern nano-optics, photonics and plasmonics, these phenomena crucially determine the behaviour of light. This is why the optical SOI are attracting such rapidly growing interest.

The SOI of light have both fundamental and applied importance for physics. On the one hand, these phenomena allow the direct observation of fundamental spin-induced effects in the dynamics of relativistic spinning particles (photons). Measurements of similar effects, for example, for Dirac electrons or analogous condensed-matter quasiparticles, are far beyond current capabilities. On the other hand, akin to the significant enhancement of electron SOI in solid-state crystals, the SOI of light are considerably enhanced by material anisotropies and can be artificially designed in optical nanostructures, including metamaterials. This paves the way to spinoptics: an optical counterpart of electron spintronics in solids. Introducing additional spin degrees of freedom for the smart control of light promises important applications in photonics, optical communications, metrology and quantum information processing. In this manner, the SOI of light conform to the most important trends in modern engineering: miniaturization of devices down to subwavelength scales, and increasing the amount of information available through additional internal degrees of freedom.

Examples shown throughout this Review clearly show that SOI phenomena can play diverse roles across various optical systems. On the one hand, they are inevitably present as small wavelength-scale aberrations in any optical interface or lens (Figs 1,2), which means these effects must be taken into account in all precision devices. On the other hand, they can dramatically affect and control the intensity and propagation of light in inhomogeneous fields and structured media. Moreover, because SOI phenomena are usually determined by basic symmetry properties and are robust with respect to perturbations in the system, it is natural to employ these phenomena for the spin-dependent shaping and control of light. In particular, Figs 2–4 show examples of how one can introduce spin control in the following fundamental processes: optical manipulation of small particles; zero-to-maximum intensity switching; subwavelength optical probing; directional propagation and diffraction; generation of vortex beams; propagation and spectrum of Bloch modes in metamaterials; and the unidirectional excitation of surface and waveguide modes.

The SOI of light therefore represent an important and integral part of modern optics. We hope this Review will aid further progress in this rapidly advancing area by forming an effective framework for future studies and applications of optical spin-orbit phenomena.

Received 18 June 2015; accepted 22 September 2015; published online 27 November 2015

References

1. Born, M. & Wolf, E. *Principles of Optics* (Pergamon, 2005).
2. Akhiezer, A. I. & Berestetskii, V. B. *Quantum Electrodynamics* (Interscience Publishers, 1965).
3. Liberman, V. S. & Zel'dovich, B. Y. Spin-orbit interaction of a photon in an inhomogeneous medium. *Phys. Rev. A* **46,** 5199–5207 (1992).
4. Bliokh, K. Y., Aiello, A. & Alonso, M. A. in *The Angular Momentum of Light* (eds. Andrews, D. L. & Babiker, M.) 174–245 (Cambridge Univ. Press, 2012).
5. Hasman, E., Biener, G., Niv, A. & Kleiner, V. Space-variant polarization manipulation. *Prog. Opt.* **47,** 215–289 (2005).
6. Marrucci, L. *et al.* Spin-to-orbital conversion of the angular momentum of light and its classical and quantum applications. *J. Opt.* **13,** 064001 (2011).
7. Bliokh, K. Y. Geometrodynamics of polarized light: Berry phase and spin Hall effect in a gradient-index medium. *J. Opt. A* **11,** 094009 (2009).
8. Bliokh, K. Y., Alonso, M. A., Ostrovskaya, E. A. & Aiello, A. Angular momenta and spin-orbit interaction of nonparaxial light in free space. *Phys. Rev. A* **82,** 063825 (2010).
9. Mathur, H. Thomas precession, spin-orbit interaction, and Berry's phase. *Phys. Rev. Lett.* **67,** 3325–3327 (1991).
10. Bérard, A. & Mohrbach, H. Spin Hall effect and Berry phase of spinning particles. *Phys. Lett. A* **352,** 190–195 (2006).
11. Rashba, E. I. Spin-orbit coupling and spin transport. *Phys. E* **34,** 31–35 (2006).
12. Xiao, D., Chang, M.-C. & Niu, Q. Berry phase effects on electronic properties. *Rev. Mod. Phys.* **82,** 1959–2007 (2010).
13. Bliokh, K. Y. & Bliokh, Y. P. Topological spin transport of photons: The optical Magnus effect and Berry phase. *Phys. Lett. A* **333,** 181–186 (2004).
14. Onoda, M., Murakami, S. & Nagaosa, N. Hall effect of light. *Phys. Rev. Lett.* **93,** 083901 (2004).
15. Bliokh, K. Y. & Bliokh, Y. P. Conservation of angular momentum, transverse shift, and spin Hall effect in reflection and refraction of an electromagnetic wave packet. *Phys. Rev. Lett.* **96,** 073903 (2006).
16. Hosten, O. & Kwiat, P. Observation of the spin Hall effect of light via weak measurements. *Science* **319,** 787–790 (2008).
17. Aiello, A. & Woerdman, J. P. Role of beam propagation in Goos–Hänchen and Imbert–Fedorov shifts. *Opt. Lett.* **33,** 1437–1439 (2008).
18. Bliokh, K. Y., Niv, A., Kleiner, V. & Hasman, E. Geometrodynamics of spinning light. *Nature Photon.* **2,** 748–753 (2008).
19. Bliokh, K. Y. & Aiello, A. Goos–Hänchen and Imbert–Fedorov beam shifts: An overview. *J. Opt.* **15,** 014001 (2013).
20. Gorodetski, Y. *et al.* Weak measurements of light chirality with a plasmonic slit. *Phys. Rev. Lett.* **109,** 013901 (2012).
21. Zhou, X., Xiao, Z., Luo, H. & Wen, S. Experimental observation of the spin Hall effect of light on a nanometal film via weak measurements. *Phys. Rev. A* **85,** 043809 (2012).
22. Zhou, X., Ling, X., Luo, H. & Wen, S. Identifying graphene layers via spin Hall effect of light. *Appl. Phys. Lett.* **101,** 251602 (2012).
23. Bokor, N., Iketaki, Y., Watanabe, T. & Fujii, M. Investigation of polarization effects for high-numerical-aperture first-order Laguerre–Gaussian beams by 2D scanning with a single fluorescent microbead. *Opt. Express* **13,** 10440–10447 (2005).
24. Dogariu, A. & Schwartz, C. Conservation of angular momentum of light in single scattering. *Opt. Express* **14,** 8425–8433 (2006).
25. Adachi, H., Akahoshi, S. & Miyakawa, K. Orbital motion of spherical microparticles trapped in diffraction patterns of circularly polarized light. *Phys. Rev. A* **75,** 063409 (2007).
26. Zhao, Y., Edgar, J. S., Jeffries, G. D. M., McGloin, D. & Chiu, D. T. Spin-to-orbital angular momentum conversion in a strongly focused optical beam. *Phys. Rev. Lett.* **99,** 073901 (2007).
27. Nieminen, T. A., Stilgoe, A. B., Heckenberg, N. R. & Rubinsztein-Dunlop, H. Angular momentum of a strongly focused Gaussian beam. *J. Opt. A* **10,** 115005 (2008).
28. Bomzon, Z. & Gu, M. Space-variant geometrical phases in focused cylindrical light beams. *Opt. Lett.* **32,** 3017–3019 (2007).
29. Gorodetski, Y., Niv, A., Kleiner, V. & Hasman, E. Observation of the spin-based plasmonic effect in nanoscale structures. *Phys. Rev. Lett.* **101,** 043903 (2008).
30. Haefner, D., Sukhov, S. & Dogariu, A. Spin Hall effect of light in spherical geometry. *Phys. Rev. Lett.* **102,** 123903 (2009).
31. Bliokh, K. Y. *et al.* Spin-to-orbit angular momentum conversion in focusing, scattering, and imaging systems. *Opt. Express* **19,** 26132–26149 (2011).
32. Baranova, N. B., Savchenko, A. Y. & Zel'dovich, B. Y. Transverse shift of a focal spot due to switching of the sign of circular-polarization. *JETP Lett.* **59,** 232–234 (1994).
33. Zel'dovich, B. Y., Kundikova, N. D. & Rogacheva, L. F. Observed transverse shift of a focal spot upon a change in the sign of circular polarization. *JETP Lett.* **59,** 766–769 (1994).
34. Bliokh, K. Y., Gorodetski, Y., Kleiner, V. & Hasman, E. Coriolis effect in optics: Unified geometric phase and spin-Hall effect. *Phys. Rev. Lett.* **101,** 030404 (2008).
35. Rodríguez-Herrera, O. G., Lara, D., Bliokh, K. Y., Ostrovskaya, E. A. & Dainty, C. Optical nanoprobing via spin-orbit interaction of light. *Phys. Rev. Lett.* **104,** 253601 (2010).
36. Ling, X. *et al.* Realization of tunable spin-dependent splitting in intrinsic photonic spin Hall effect. *Appl. Phys. Lett.* **105,** 151101 (2014).
37. Kruk, S. S. *et al.* Spin-polarized photon emission by resonant multipolar nanoantennas. *ACS Photon.* **1,** 1218–1223 (2014).
38. Van Enk, S. J. & Nienhuis, G. Commutation rules and eigenvalues of spin and orbital angular momentum of radiation fields. *J. Mod. Opt.* **41,** 963–977 (1994).
39. Roy, B., Ghosh, N., Banerjee, A., Gupta, S. D. & Roy, S. Enhanced topological phase and spin Hall shifts in an optical trap. *New J. Phys.* **16,** 083037 (2013).
40. Hielscher, A. *et al.* Diffuse backscattering Mueller matrices of highly scattering media. *Opt. Express* **1,** 441–453 (1997).
41. Schwartz, C. & Dogariu, A. Backscattered polarization patterns, optical vortices, and the angular momentum of light. *Opt. Lett.* **31,** 1121–1123 (2006).
42. Gorodetski, Y., Shitrit, N., Bretner, I., Kleiner, V. & Hasman, E. Observation of optical spin symmetry breaking in nanoapertures. *Nano Lett.* **9,** 3016–3019 (2009).
43. Vuong, L. T., Adam, A. J. L., Brok, J. M., Planken, P. C. M. & Urbach, H. P. Electromagnetic spin-orbit interactions via scattering of subwavelength apertures. *Phys. Rev. Lett.* **104,** 083903 (2010).

44. Darsht, M. Y., Zel'dovich, B. Y., Kataevskaya, I. V. & Kundikova, N. D. Formation of an isolated wavefront dislocation. *JETP* **80,** 817–821 (1995).
45. Ciattoni, A., Cincotti, G. & Palma, C. Angular momentum dynamics of a paraxial beam in a uniaxial crystal. *Phys. Rev. E* **67,** 36618 (2003).
46. Brasselet, E. *et al.* Dynamics of optical spin-orbit coupling in uniaxial crystals. *Opt. Lett.* **34,** 1021–1023 (2009).
47. Berry, M. V, Jeffrey, M. R. & Mansuripur, M. Orbital and spin angular momentum in conical diffraction. *J. Opt. A* **7,** 685–690 (2005).
48. Bomzon, Z., Biener, G., Kleiner, V. & Hasman, E. Space-variant Pancharatnam–Berry phase optical elements with computer-generated subwavelength gratings. *Opt. Lett.* **27,** 1141–1143 (2002).
49. Biener, G., Niv, A., Kleiner, V. & Hasman, E. Formation of helical beams by use of Pancharatnam–Berry phase optical elements. *Opt. Lett.* **27,** 1875–1877 (2002).
50. Marrucci, L., Manzo, C. & Paparo, D. Optical spin-to-orbital angular momentum conversion in inhomogeneous anisotropic media. *Phys. Rev. Lett.* **96,** 163905 (2006).
51. Brasselet, E., Murazawa, N., Misawa, H. & Juodkazis, S. Optical vortices from liquid crystal droplets. *Phys. Rev. Lett.* **103,** 103903 (2009).
52. Shitrit, N., Bretner, I., Gorodetski, Y., Kleiner, V. & Hasman, E. Optical spin Hall effects in plasmonic chains. *Nano Lett.* **11,** 2038–2042 (2011).
53. Huang, L. *et al.* Helicity dependent directional surface plasmon polariton excitation using a metasurface with interfacial phase discontinuity. *Light Sci. Appl.* **2,** e70 (2013).
54. Lin, J. *et al.* Polarization-controlled tunable directional coupling of surface plasmon polaritons. *Science* **340,** 331–334 (2013).
55. Shitrit, N. *et al.* Spin-optical metamaterial route to spin-controlled photonics. *Science* **340,** 724–726 (2013).
56. Yu, N. & Capasso, F. Flat optics with designer metasurfaces. *Nature Mater.* **13,** 139–150 (2014).
57. Veksler, D. *et al.* Multiple wavefront shaping by metasurface based on mixed random antenna groups. *ACS Photon.* **2,** 661–667 (2015).
58. Lee, S.-Y. *et al.* Role of magnetic induction currents in nanoslit excitation of surface plasmon polaritons. *Phys. Rev. Lett.* **108,** 213907 (2012).
59. Rodríguez-Fortuño, F. J. *et al.* Near-field interference for the unidirectional excitation of electromagnetic guided modes. *Science* **340,** 328–330 (2013).
60. Petersen, J., Volz, J. & Rauschenbeutel, A. Chiral nanophotonic waveguide interface based on spin-orbit interaction of light. *Science* **346,** 67–71 (2014).
61. O'Connor, D., Ginzburg, P., Rodríguez-Fortuño, F. J., Wurtz, G. A. & Zayats, A. V. Spin–orbit coupling in surface plasmon scattering by nanostructures. *Nature Commun.* **5,** 5327 (2014).
62. Mitsch, R., Sayrin, C., Albrecht, B., Schneeweiss, P. & Rauschenbeutel, A. Quantum state-controlled directional spontaneous emission of photons into a nanophotonic waveguide. *Nature Commun.* **5,** 5713 (2014).
63. Le Feber, B., Rotenberg, N. & Kuipers, L. Nanophotonic control of circular dipole emission. *Nature Commun.* **6,** 6695 (2015).
64. Söllner, I. *et al.* Deterministic photon–emitter coupling in chiral photonic circuits. *Nature Nanotechnol.* **10,** 775–778 (2015).
65. Kapitanova, P. V. *et al.* Photonic spin Hall effect in hyperbolic metamaterials for polarization-controlled routing of subwavelength modes. *Nature Commun.* **5,** 3226 (2014).
66. Bliokh, K. Y. & Nori, F. Transverse spin of a surface polariton. *Phys. Rev. A* **85,** 061801(R) (2012).
67. Bliokh, K. Y., Bekshaev, A. Y. & Nori, F. Extraordinary momentum and spin in evanescent waves. *Nature Commun.* **5,** 3300 (2014).
68. Bliokh, K. Y., Smirnova, D. & Nori, F. Quantum spin Hall effect of light. *Science* **348,** 1448–1451 (2015).
69. Lu, L., Joannopoulos, J. D. & Soljačić, M. Topological photonics. *Nature Photon.* **8,** 821–829 (2014).
70. Pichler, H., Ramos, T., Daley, A. J. & Zoller, P. Quantum optics of chiral spin networks. *Phys. Rev. A* **91,** 042116 (2015).
71. Sayrin, C. *et al.* Optical diode based on the chirality of guided photons. Preprint at http://arxiv.org/abs/1502.01549 (2015).
72. Allen, L., Barnett, S. M. & Padgett, M. J. *Optical Angular Momentum* (IOP, 2003).
73. Andrews, D. L. & Babiker, M. *The Angular Momentum of Light* (Cambridge Univ. Press, 2013).
74. Bliokh, K. Y. & Nori, F. Transverse and longitudinal angular momenta of light. *Phys. Rep.* **592,** 1–38 (2015).
75. Vinitskii, S. I., Derbov, V. L., Dubovik, V. M., Markovski, B. L. & Stepanovskii, Y. P. Topological phases in quantum mechanics and polarization optics. *Uspekhi Fiz. Nauk* **33,** 403–428 (1990).
76. Bhandari, R. Polarization of light and topological phases. *Phys. Rep.* **281,** 1–64 (1997).
77. Alexeyev, C. N. & Yavorsky, M. A. Topological phase evolving from the orbital angular momentum of 'coiled' quantum vortices. *J. Opt. A* **8,** 752–758 (2006).
78. Bliokh, K. Y. Geometrical optics of beams with vortices: Berry phase and orbital angular momentum Hall effect. *Phys. Rev. Lett.* **97,** 043901 (2006).
79. Bialynicki-Birula, I. & Bialynicka-Birula, Z. Berrys phase in the relativistic theory of spinning particles. *Phys. Rev. D* **35,** 2383–2387 (1987).
80. Kravtsov, Y. A. & Orlov, Y. I. *Geometrical Optics of Inhomogeneous Media* (Springer, 1990).
81. Duval, C., Horváth, Z. & Horváthy, P. A. Fermat principle for spinning light. *Phys. Rev. D* **74,** 021701(R) (2006).
82. Chiao, R. Y. & Wu, Y. S. Manifestations of Berry's topological phase for the photon. *Phys. Rev. Lett.* **57,** 933–936 (1986).
83. Tomita, A. & Chiao, R. Observation of Berry's topological phase by use of an optical fiber. *Phys. Rev. Lett.* **57,** 937–940 (1986).
84. Murakami, S., Nagaosa, N. & Zhang, S.-C. Dissipationless quantum spin current at room temperature. *Science* **301,** 1348–1351 (2003).
85. Wunderlich, J., Kaestner, B., Sinova, J. & Jungwirth, T. Experimental observation of the spin-Hall effect in a two-dimensional spin-orbit coupled semiconductor system. *Phys. Rev. Lett.* **94,** 047204 (2005).
86. Bliokh, K. Y. & Bliokh, Y. P. Polarization, transverse shifts, and angular momentum conservation laws in partial reflection and refraction of an electromagnetic wave packet. *Phys. Rev. E* **75,** 066609 (2007).
87. Fedorov, F. I. To the theory of total reflection. *J. Opt.* **15,** 014002 (2013).
88. Imbert, C. Calculation and experimental proof of the transverse shift induced by total internal reflection of a circularly polarized light beam. *Phys. Rev. D* **5,** 787–796 (1972).
89. Dennis, M. R. & Götte, J. B. The analogy between optical beam shifts and quantum weak measurements. *New J. Phys.* **14,** 073013 (2012).
90. Götte, J. B. & Dennis, M. R. Limits to superweak amplification of beam shifts. *Opt. Lett.* **38,** 2295–2297 (2013).
91. Player, M. A. Angular momentum balance and transverse shifts on reflection of light. *J. Phys. A. Math. Gen.* **20,** 3667–3678 (1987).
92. Fedoseyev, V. G. Conservation laws and transverse motion of energy on reflection and transmission of electromagnetic waves. *J. Phys. A. Math. Gen.* **21,** 2045–2059 (1988).
93. Aiello, A., Merano, M. & Woerdman, J. P. Duality between spatial and angular shift in optical reflection. *Phys. Rev. A* **80,** 061801(R) (2009).
94. Hermosa, N., Nugrowati, A. M., Aiello, A. & Woerdman, J. P. Spin Hall effect of light in metallic reflection. *Opt. Lett.* **36,** 3200–3202 (2011).
95. Qin, Y. *et al.* Spin Hall effect of reflected light at the air-uniaxial crystal interface. *Opt. Express* **18,** 16832–16839 (2010).
96. Ménard, J.-M., Mattacchione, A., van Driel, H., Hautmann, C. & Betz, M. Ultrafast optical imaging of the spin Hall effect of light in semiconductors. *Phys. Rev. B* **82,** 045303 (2010).
97. Yin, X., Ye, Z., Rho, J., Wang, Y. & Zhang, X. Photonic spin Hall effect at metasurfaces. *Science* **339,** 1405–1407 (2013).
98. Qin, Y., Li, Y., He, H. & Gong, Q. Measurement of spin Hall effect of reflected light. *Opt. Lett.* **34,** 2551–2553 (2009).
99. Luo, H., Zhou, X., Shu, W., Wen, S. & Fan, D. Enhanced and switchable spin Hall effect of light near the Brewster angle on reflection. *Phys. Rev. A* **84,** 043806 (2011).
100. Qin, Y. *et al.* Observation of the in-plane spin separation of light. *Opt. Express* **19,** 9636–9645 (2011).
101. Fedoseyev, V. G. Spin-independent transverse shift of the centre of gravity of a reflected and of a refracted light beam. *Opt. Commun.* **193,** 9–18 (2001).
102. Dasgupta, R. & Gupta, P. K. Experimental observation of spin-independent transverse shift of the centre of gravity of a reflected Laguerre–Gaussian light beam. *Opt. Commun.* **257,** 91–96 (2006).
103. Okuda, H. & Sasada, H. Huge transverse deformation in nonspecular reflection of a light beam possessing orbital angular momentum near critical incidence. *Opt. Express* **14,** 8393–8402 (2006).
104. Bliokh, K. Y., Shadrivov, I. V & Kivshar, Y. S. Goos–Hänchen and Imbert–Fedorov shifts of polarized vortex beams. *Opt. Lett.* **34,** 389–391 (2009).
105. Merano, M., Hermosa, N., Woerdman, J. P. & Aiello, A. How orbital angular momentum affects beam shifts in optical reflection. *Phys. Rev. A* **82,** 023817 (2010).
106. Dennis, M. R. & Götte, J. B. Topological aberration of optical vortex beams: Determining dielectric interfaces by optical singularity shifts. *Phys. Rev. Lett.* **109,** 183903 (2012).
107. Li, C. F. Spin and orbital angular momentum of a class of nonparaxial light beams having a globally defined polarization. *Phys. Rev. A* **80,** 063814 (2009).
108. Monteiro, P. B., Neto, P. A. M. & Nussenzveig, H. M. Angular momentum of focused beams: Beyond the paraxial approximation. *Phys. Rev. A* **79,** 033830 (2009).
109. Zhao, Y., Shapiro, D., McGloin, D., Chiu, D. T. & Marchesini, S. Direct observation of the transfer of orbital angular momentum to metal particles from a focused circularly polarized Gaussian beam. *Opt. Express* **17,** 23316–23322 (2009).

110. Richards, B. & Wolf, E. Electromagnetic diffraction in optical systems. II. Structure of the image field in an aplanatic system. *Proc. R. Soc. A Math. Phys. Eng. Sci.* **253,** 358–379 (1959).
111. O'Neil, A. T., MacVicar, I., Allen, L. & Padgett, M. J. Intrinsic and extrinsic nature of the orbital angular momentum of a light beam. *Phys. Rev. Lett.* **88,** 053601 (2002).
112. Garcés-Chávez, V. *et al.* Observation of the transfer of the local angular momentum density of a multiringed light beam to an optically trapped particle. *Phys. Rev. Lett.* **91,** 093602 (2003).
113. Curtis, J. E. & Grier, D. G. Structure of optical vortices. *Phys. Rev. Lett.* **90,** 133901 (2003).
114. Zambrana-Puyalto, X., Vidal, X. & Molina-Terriza, G. Angular momentum-induced circular dichroism in non-chiral nanostructures. *Nature Commun.* **5,** 4922 (2014).
115. Moe, G. & Happer, W. Conservation of angular momentum for light propagating in a transparent anisotropic medium. *J. Phys. B* **10,** 1191–1208 (2001).
116. Gorodetski, Y., Nechayev, S., Kleiner, V. & Hasman, E. Plasmonic Aharonov–Bohm effect: Optical spin as the magnetic flux parameter. *Phys. Rev. B* **82,** 125433 (2010).
117. Lacoste, D., Rossetto, V., Jaillon, F. & Saint-Jalmes, H. Geometric depolarization in patterns formed by backscattered light. *Opt. Lett.* **29,** 2040–2042 (2004).
118. Kobayashi, H., Nonaka, K. & Kitano, M. Helical mode conversion using conical reflector. *Opt. Express* **20,** 14064 (2012).
119. Berry, M. V. Lateral and transverse shifts in reflected dipole radiation. *Proc. R. Soc. A Math. Phys. Eng. Sci.* **467,** 2500–2519 (2011).
120. Garbin, V. *et al.* Mie scattering distinguishes the topological charge of an optical vortex: A homage to Gustav Mie. *New J. Phys.* **11,** 013046 (2009).
121. Litchinitser, N. M. Structured light meets structured matter. *Science* **337,** 1054–1055 (2012).
122. Hasman, E., Bomzon, Z., Niv, A., Biener, G. & Kleiner, V. Polarization beam-splitters and optical switches based on space-variant computer-generated subwavelength quasi-periodic structures. *Opt. Commun.* **209,** 45–54 (2002).
123. Lin, D., Fan, P., Hasman, E. & Brongersma, M. L. Dielectric gradient metasurface optical elements. *Science* **345,** 298–302 (2014).
124. Li, G. *et al.* Spin-enabled plasmonic metasurfaces for manipulating orbital angular momentum of light. *Nano Lett.* **13,** 4148–4151 (2013).
125. Xiao, S., Zhong, F., Liu, H., Zhu, S. & Li, J. Flexible coherent control of plasmonic spin-Hall effect. *Nature Commun.* **6,** 8360 (2015).
126. Nagali, E. *et al.* Quantum information transfer from spin to orbital angular momentum of photons. *Phys. Rev. Lett.* **103,** 013601 (2009).
127. Slussarenko, S. *et al.* Tunable liquid crystal q-plates with arbitrary topological charge. *Opt. Express* **19,** 4085–4090 (2011).
128. Khilo, N. A., Petrova, E. S. & Ryzhevich, A. A. Transformation of the order of Bessel beams in uniaxial crystals. *Quantum Electron.* **31,** 85–89 (2001).
129. Beth, R. A. Mechanical detection and measurement of the angular momentum of light. *Phys. Rev.* **50,** 115–125 (1936).
130. Hakobyan, D. & Brasselet, E. Left-handed optical radiation torque. *Nature Photon.* **8,** 610–614 (2014).
131. Yang, S., Chen, W., Nelson, R. L. & Zhan, Q. Miniature circular polarization analyzer with spiral plasmonic lens. *Opt. Lett.* **34,** 3047–3049 (2009).
132. Kim, H. *et al.* Synthesis and dynamic switching of surface plasmon vortices with plasmonic vortex lens. *Nano Lett.* **10,** 529–536 (2010).
133. Dahan, N., Gorodetski, Y., Frischwasser, K., Kleiner, V. & Hasman, E. Geometric Doppler effect: Spin-split dispersion of thermal radiation. *Phys. Rev. Lett.* **105,** 136402 (2010).
134. Rodríguez-Fortuño, F. J., Barber-Sanz, I., Puerto, D., Griol, A. & Martinez, A. Resolving light handedness with an on-chip silicon microdisk. *ACS Photon.* **1,** 762–767 (2014).
135. Young, A. B. *et al.* Polarization engineering in photonic crystal waveguides for spin-photon entanglers. *Phys. Rev. Lett.* **115,** 153901 (2015).
136. Lefier, Y. & Grosjean, T. Unidirectional sub-diffraction waveguiding based on optical spin-orbit coupling in subwavelength plasmonic waveguides. *Opt. Lett.* **40,** 2890–2893 (2015).
137. Hasan, M. Z. & Kane, C. L. Colloquium: Topological insulators. *Rev. Mod. Phys.* **82,** 3045–3067 (2010).
138. Garetz, B. A. & Arnold, S. Variable frequency shifting of circularly polarized laser radiation via a rotating half-wave retardation plate. *Opt. Commun.* **31,** 1–3 (1979).
139. Garetz, B. A. Angular Doppler effect. *J. Opt. Soc. Am.* **71,** 609–611 (1981).
140. Mashhoon, B. Neutron interferometry in a rotating frame of reference. *Phys. Rev. Lett.* **61,** 2639–2642 (1988).
141. Lipson, S. G. Berry's phase in optical interferometry: A simple derivation. *Opt. Lett.* **15,** 154–155 (1990).
142. Shitrit, N. *et al.* Spinoptical metamaterials: A novel class of metasurfaces. *Opt. Photon. News* 53 (December 2013).

Acknowledgements

This work was partially supported by the RIKEN iTHES Project, MURI Center for Dynamic Magneto-Optics (AFOSR grant no. FA9550-14-1-0040), JSPS-RFBR (contract no. 12-02-92100), Grant-in-Aid for Scientific Research (A), the Australian Research Council, EPSRC (UK), and the ERC iPLASMM project (321268). A.V.Z. acknowledges support from the Royal Society and the Wolfson Foundation.

Author contributions

K.Y.B. wrote the major part of the text, with the input from F.J.R.F., F.N., and A.V.Z. F.J.R.F. created most of the figures with the input from K.Y.B. F.N. and A.V.Z. helped with the writing and contributed to discussions.

Additional information

Reprints and permissions information is available online at www.nature.com/reprints. Correspondence should be addressed to K.Y.B.

Competing financial interests

The authors declare no competing financial interests.